remote sensing

MDPI

Article

New Inventories of Global Carbon Dioxide Emissions through Biomass Burning in 2001–2020

Tomohiro Shiraishi [1,*], Ryuichi Hirata [1] and Takashi Hirano [2]

[1] Center for Global Environmental Research, Earth System Division, National Institute for Environmental Studies, 16-1 Onogawa, Tsukuba, Ibaraki 305-8506, Japan; hirata.ryuichi@nies.go.jp

[2] Research Faculty of Agriculture, Hokkaido University, Kita 9, Nishi 9, Kita-ku, Sapporo, Hokkaido 060-8589, Japan; hirano@env.agr.hokudai.ac.jp

* Correspondence: shiraishi.tomohiro@nies.go.jp

Abstract: Recently, the effect of large-scale fires on the global environment has attracted attention. Satellite observation data are used for global estimation of fire CO_2 emissions, and available data sources are increasing. Although several CO_2 emission inventories have already been released, various remote sensing data were used to create the inventories depend on the studies. We created eight global CO_2 emission inventories through fires from 2001 to 2020 by combining input data sources, compared them with previous studies, and evaluated the effect of input sources on CO_2 emission estimation. CO_2 emissions were estimated using a method that combines the biomass density change (by the repeated fires) with the general burned area approach. The average annual CO_2 emissions of the created eight inventories were 8.40 $\pm$ 0.70 Pg CO_2 year^{-1} ($\pm$1 standard deviation), and the minimum and maximum emissions were 3.60 $\pm$ 0.67 and 14.5 $\pm$ 0.83 Pg CO_2 year^{-1}, respectively, indicating high uncertainty. CO_2 Emissions obtained from four previous inventories were within $\pm$1 standard deviation in the eight inventories created in this study. Input datasets, especially biomass density, affected CO_2 emission estimation. The global annual CO_2 emissions from two biomass maps differed by 60% (Maximum). This study assesses the performance of climate and fire models by revealing the uncertainty of fire emission estimation from the input sources.

Keywords: CO_2 emissions; biomass burning; fire map; land cover map; above-ground biomass map

check for updates

Citation: Shiraishi, T.; Hirata, R.; Hirano, T. New Inventories of Global Carbon Dioxide Emissions through Biomass Burning in 2001–2020. *Remote Sens.* **2021**, *13*, 1914. https://doi.org/10.3390/rs13101914

Academic Editor: Michael Obland

Received: 12 March 2021
Accepted: 11 May 2021
Published: 13 May 2021

1. Introduction

Biomass burning occurs in all vegetated terrestrial ecosystems and strongly affects global carbon cycles through a huge amount of carbon dioxide (CO_2) in the atmosphere (e.g., [1–6]). The largest source of global carbon emissions, excluding fossil fuel emissions, is fires, mainly in grasslands and savannas; fires in those areas combining with woodlands account for 60% of total global fire emissions [5]. In South America, approximately half of carbon emissions from deforestation and forest degradation are due to fires [7,8], including anthropogenic fires that convert forests to farmlands and pastures [9]. Lightning strikes are important ignition causes in boreal regions [2].

Research on how biomass burning affects atmospheric trace gases and aerosols began in the late 1970s [10]. Currently, studies on fire CO_2 emissions have expanded to a global scale [11]. These studies include extensive and frequent estimates of fire emissions using satellite data [12,13]. In addition, several global fire emissions inventories have been developed. One of the inventories is the global fire emissions database (GFED) with a spatial resolution of 0.25-degrees and 3-h temporal resolution. In GFED, fire emissions of trace gas species, such as CO_2, carbon monoxide (CO), methane (CH_4), etc., are estimated using the Carnegie Ames Stanford approach (CASA) biogeochemical model, and GFED uses NASA's moderate resolution imaging spectroradiometer (MODIS) MCD64A1 product for the burned area, MCD12C1 for land cover types, and GEOCARBON biomass map [14,15] to adjust biomass in the carbon pool of CASA model [4–6,16]. The global fire assimilation system (GFAS) is another emissions inventory with 0.1-degree spatial resolution and daily temporal resolution. GFAS is based on burned area detected by fire radiative power (FRP) of MODIS MOD14 product, in which the burned area is used to predict CO_2 emissions in the integrated forecasting system model of the European Centre for Medium-Range Weather Forecasts and uses organic soil and peat maps from GFED3.1 [2,17,18]. The fire inventory from the National Center for Atmospheric Research (FINN) provides fire emissions inventory with 1-km spatial resolution on a daily basis, in which fire emissions are calculated as a function of burned area, biomass density, biomass burning rates, and emission factors: MODIS MOD14 product for burned area, the global land cover 2000 project (GLC2000) [19,20] for land cover types, and a fixed value assigned to each land cover category for biomass density [21,22]. Global Inventory for Chemistry-Climate studies (GICC) is an inventory with 1-degree spatial resolution and monthly temporal resolution, which estimates fire emissions using ASTER World Fire Atlas [23] for the burned area, GBA2000 [24] land cover product, fixed values for biomass density, biomass burning rates, and emission factors [25]. The GICC-GFED4 (G-G) is an inventory with a spatial resolution of 0.25-degrees and monthly temporal resolution based on GICC using GFED4 for the burned area, GLC2000 for land cover, and fixed values for biomass density [26]. Fire emission uncertainty is high in each inventory despite the aforementioned effort (e.g., [6,17,22,25]), including uncertainties arising from fixed emission factors assigned for each land cover category. Thus, fire emission inventories have room for improvement.

It is challenging to verify the accuracy of an inventory estimated from satellite observation data because direct measurement of CO_2 emissions from fires is difficult. In the conventional burned area approach using satellite data, fire CO_2 emissions are estimated from burned area, land cover type, biomass density, burning efficiency, and emission factor. However, because each data source contains uncertainties, it is necessary to improve the accuracy of each component to increase the total accuracy of the CO_2 emission estimations. Although various data sources were used in previous studies, the effects of input sources on the CO_2 emission estimation are unclear. This study aims to reveal the uncertainty of the fire emission estimation by input sources. This study covers the following: (1) provides eight global CO_2 emission inventories through fires; (2) quantifies the effect of the CO_2 emission estimation by input sources; (3) compares with four previous studies. It is important to reduce the uncertainty of fire emission estimation to understand the global environment. This study helps to assess the performance of climate and fire models. The abbreviation list in this paper is shown in Table S1.

2. Materials and Methods

2.1. Maps and Datasets

The remote sensing products of fire distribution (FD), land cover classification (LCC), and above-ground biomass (AGB) were used to estimate CO_2 emissions through fires. The datasets used were selected from the products that were used in previous studies with global and long-term observation data. The remote sensing datasets were resampled at 500 m spatial resolution to equalize the spatial positions of the three global maps using the NEAREST function in ArcGIS version 5.1 because the datasets have different spatial resolutions.

2.1.1. FD Maps

FD maps are used to obtain the burned areas and the number of fire occurrences monthly and yearly. The Thermal Anomalies and Fire MODIS data product version 6 (MOD14A1) was used to determine the global burned area [27,28]. MOD14A1 is a daily fire data product with a 1-km spatial resolution at intervals of eight days. Every fire pixel is assigned as having either low (0% to 30%), nominal (30% to 80%), or high (80% to 100%) confidence levels [29]. We created three types of FD maps with data on the number of fire occurrences, depending on the confidence level: HC-M with 80% to 100% confidence level was created from high confidence flag, NC-M with 30% to 100% confidence level created from high and nominal confidence flags, and LC-M with 0% to 100% confidence level was created from high, nominal, and low confidence flags on MOD14A1. The number of fire occurrences in the FD maps was counted depending on the confidence level in each map on the same grid position on a monthly or yearly basis. All ongoing fire on the same grid position in the MOD14A1 daily datasets is a single fire.

2.1.2. LCC Maps

LCC maps are used to determine the scaling factors (burning efficiency and emission factor) using the land cover category on the burned area. The MODIS Land Cover Type (MCD12Q1) Version 6 data product [30,31] and global land cover 2000 project (GLC2000) data product [19,20] were used to obtain the appropriate scaling factors, which are burning efficiency (BE) and emission factor (EF), for each land cover category, the same with GICC [25] and G-G [26]. MCD12Q1 produced using ground surface reflectance data observed using MODIS instruments aboard NASA's Terra and Aqua satellites, is the global annual LCC map from 2001 to 2018 having 500-m spatial resolution. We used the International Geosphere-Biosphere Program land cover type with 17 categories in five land cover types in MCD12Q1. GLC2000 is a global LCC map, which was produced using data acquired using the VEGETATION instrument aboard the SPOT 4 satellite in 2000, with a 1-km spatial resolution and 22 land cover types based on the food and agriculture organization land cover classification system. MCD12Q1 of 2019 was a used to estimate the CO_2 emissions for 2020 because the 2020 datasets were not published at the time of the study.

2.1.3. AGB Maps

ABG maps are used to determine the AGB density on the burned area. GICC and G-G used a fixed biomass density for each land cover category. However, we used the up-to-date biomass maps of the GEOCARBON global forest biomass [14,15] and Globbiomass AGB maps [32]. GEOCARBON map, which combined AGB maps of Saatchi et al. (2011) [33] and Baccini et al. (2012) [34], is a global AGB map with a 1-km spatial resolution that uses an independent reference dataset of field observations and locally calibrated biomass map [15]. Globbiomass is a global AGB map with a 25-m resolution, produced by the European Space Agency (ESA), which uses satellite observation data, such as Envisat ASAR, ALOS PALSAR, Landsat, ICESat GLAS, and MODIS Vegetation Continuous Fields [35,36].

2.2. Fire CO_2 Emissions

We created CO_2 emission inventories from fires using three types of global remote sensing data. Because the three remote sensing datasets have the same spatial region and resolution by the resampling, the LCC and AGB densities are uniquely determined depending on fire area and used as the parameters for CO_2 emissions estimation.

CO_2 emission from fires (EM, g CO_2) was conventionally calculated using a burned area approach shown in Equation (1) [25,26,37]. However, this equation cannot evaluate the number of fires occurring within a single region over a specific period. Therefore, we represented the decrease in biomass density (BD) by fires over a year by using Equation (2) to determine the above-ground BD in Equation (1), considering the number of fire occurrences, though this method does not consider annual changes in BD [38].

$$\mathrm{EM}_{(\mathrm{m,p})} = \mathrm{BA}_{(\mathrm{m,p})} \times \mathrm{BD}_{(\mathrm{m,p})} \times \mathrm{BE}_{(\mathrm{c})} \times \mathrm{EF}_{(\mathrm{c})} \tag{1}$$

$$\mathrm{BD}_{(\mathrm{m,p})} = \sum_{\mathrm{j}=\mathrm{i}+1}^{\mathrm{I}} \left\{ \mathrm{Agb}_{(\mathrm{p})} \times \left(1 - \mathrm{BE}_{(\mathrm{c})}\right)^{\mathrm{j}-1} \right\} \tag{2}$$

where m is the target month for calculating CO_2 emissions, p is the grid position on the map, c is the LCC category of the grid (p), and i and I are the cumulative numbers of fire occurrences until the preceding (m^{-1}) and target month (m), respectively, BA is the burned area (m^2), BD is the total burned biomass density (kg m^{-2}), Agb is biomass density (kg m^{-2}) from AGB map, BE is burning efficiency (0 to 1), and EF is the emission factor of dry matter (g CO_2 kg^{-1}). The BE and EF values for CO_2 emissions were from Mieville et al. (2010) [25] and Shi et al. (2015) [26], and these values for CO emissions were sourced from van der Werf et al. (2017) [6]. We assigned the BE and EF values for CO_2 emissions to fit the categories of MCD12Q1 and GLC2000 (Table S2), and those values for CO emissions are shown in Table S3 (MCD12Q1) and Table S4 (GLC2000). This estimation method for CO_2 emissions from fires does not need preprocessing, such as training of machine learning, and it is easy to implement the algorithm. Furthermore, this method is possible to respond flexibly to a change in the target region. Moreover, it is easy to modify the input datasets and scaling factors.

2.3. Data Analysis

The global burned area was annually measured with a spatial resolution of 500 m per grid for all global fires including the repeated fires on the same grid except Antarctica. To evaluate the burned area in the three FD maps, we used GFED4 and GFED4.1s, which are two versions of GFED, and CCI50, which is ESA's Climate Change Initiative program [39] in Section 3.1. GFED provides burned area products with a spatial resolution of 0.25 degrees from 1995 onward [16]. The difference between GFED4 and GFED4.1s is the inclusion of small-scale fires in GFED4.1s. CCI50 is a burned area MODIS data product with 250 m spatial resolution [16].

CO_2 emissions from fires were annually or monthly calculated for each burned grid using Equations (1) and (2) and then, integrated globally except Antarctica. Eight inventories of the CO_2 emissions were created by combining input datasets, and they were compared with each other to evaluate the effect of the inputs on the estimated emissions from 2001 to 2020, in Section 3.2. The inventories were compared to GFED4.1s, GFASv1.2, FINNv1.5, and GICC to assess their validity and variability in Section 3.3. GICC is unoriginal data but estimated CO_2 emissions from the burned area of NC-M. Scaling factors, the use of GLC2000 for LCC maps, and the estimation method are equivalent to those of Mieville et al. (2010) [25] and Shi et al. (2015) [26]. The globe was separated into 14 regions according to GFED (Figure 1), and the estimated monthly CO_2 emissions on each region were evaluated to understand the regional characteristics and variation in Section 3.4.

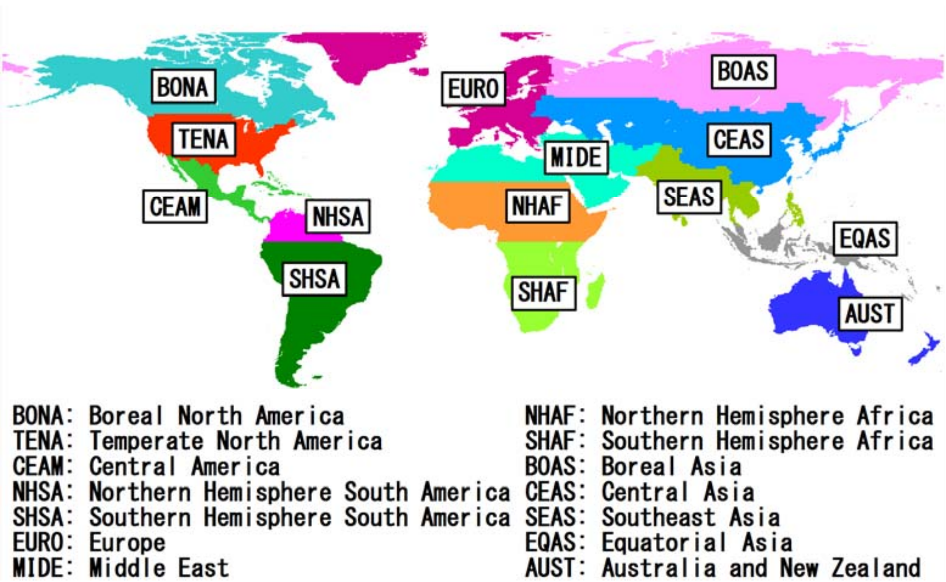

Figure 1. Spatial distribution map for the 14 evaluation regions, according to van der Werf et al. (2006) [4]. Map was created with ArcGIS version 10.5 (https://www.arcgis.com/ (accessed on 12 March 2021)).

We estimated the fire emissions by adding Equation (2), which represents the BD changes from repeated fires in the same region, to the conventional burned area approach in Equation (1). To evaluate the new CO_2 emission estimation method using Equations (1) and (2), the estimated CO_2 emissions by the method were compared with those of a general method by Equation (1) using GFED4.1s as a criterion in Section 4.5.

3. Results

3.1. Burned Area

The annual burned areas of the three FD maps are shown in Table 1 including those of GFED4.1s, GFED4, and CCI50 to compare the fire areas of the maps. The burned areas for NC-M and LC-M are 3.73 $\pm$ 0.30 and 3.92 $\pm$ 0.32 $\times$ 10^6 km^2 (mean $\pm$ 1 standard deviation (SD)), respectively; the difference is small at 0.19 $\times$ 10^6 km^2. However, the burned area of HC-M is 1.07 $\pm$ 0.11 $\times$ 10^6 km^2, which is smaller by 71–73% than those of NC-M and LC-M (Figure 2). HC-M shows that the smallest burned area in the datasets was smaller by 67% than that of GFED4. HC-M, NC-M, and LC-M were smaller by 77%, 19%, and 15%, respectively, than that of GFED4.1s. NC-M and CCI50 show similar results with a difference of 0.5%. Although CCI50 was within 1 SD of NC-M and LC-M, GFED4, and GFED4.1s were outside the SDs, respectively.

Table 1. Annual global burned area of three results (HC-M, NC-M, and LC-M) from 2001 to 2020 and three previous studies (GFED4.1s, GFED4, and CCI50) from 2001 to 2016. Numbers in parentheses are from 2001 to 2016.

Products	Period	Average (10^6 km^2)	1 Standard Deviation (10^6 km^2)
HC-M (this study)	2001–2020	1.07 (1.08)	0.11 (0.12)
NC-M (this study)	2001–2020	3.73 (3.79)	0.30 (0.31)
LC-M (this study)	2001–2020	3.92 (3.98)	0.32 (0.32)
GFED4.1s	2001–2016	4.67	0.42
GFED4	2001–2016	3.38	0.29
CCI50	2001–2016	3.80	0.29

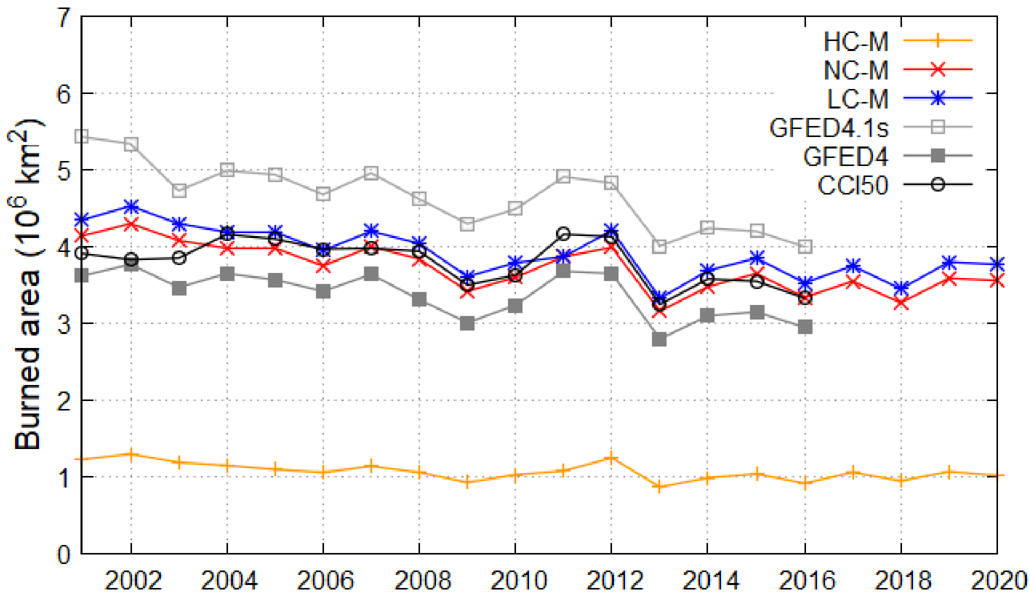

Figure 2. Interannual variation in the global burned area of the three maps of this study (HC-M, NC-M, and LC-M) and previous studies (GFED4, GFED4.1s, and CCI50) between 2001 and 2020.

The burned areas of NC-M and LC-M decreased by 14% and 13%, respectively, from 2001 to 2020. The decreasing tendencies of both burned areas were significant in the regression analysis under the confidence interval of 95% (Figure S1). In three regions (EURO, NHAF, and CEAS), the decreasing trend was statistically significant in the same analysis from 2001 to 2020 and contributed to the decreasing global burned area for NC-M and LC-M (Figure S2). Andela et al. (2017) [40] documented that the burned area decreased as the population, cultivated land, and livestock density increased in the savanna region, which has a large burned area and frequent fire occurrences. The agricultural expansion associated with human activity is an important factor for the decrease in the burned area to protect crops, livestock, and infrastructures from fires and to maintain air quality.

3.2. Global CO_2 Emissions Estimation Results

Global CO_2 emissions were estimated annually from 2001 to 2020 in eight combinations (2^3) using an FD map (NC-M or LC-M), LCC map (MCD12Q1 or GLC2000), and AGB map (GEOCARBON or Globbiomass) (Table 2 and Figure 3) to evaluate the effect of the input datasets on the CO_2 emission estimation. The annual CO_2 emission averages from 2003 to 2019 were estimated according to the analysis period of the previous studies for the comparing. The eight inventories were named using the three characters in each of the three inputs in the order of LCC (G: GLC2000 or M: MCD12Q1), AGB (W: GEOCARBON or E: Globbiomass), and FD (N: NC–M or L: LC–M) maps, for example, the MWN inventory is the combination of inputs, MCD12Q1 for LCC, GEOCARBON for AGB, and NC–M for FD (see Table 2 for every inventory). HC-M was excluded from FD maps because its burned area was smaller than those of NC-M, LC-M, and previous studies (Table 1).

Table 2. Annual global CO_2 emissions of eight inventories from 2001 to 2020. Numbers in parentheses are from 2003 to 2019.

Inventory	LCC Map	AGB Map	FD Map	Average (Pg CO_2 year^{-1})	1 Standard Deviation (Pg CO_2 year^{-1})
MWN	MCD12Q1	GEOCARBON	NC-M	6.30 (6.33)	0.67 (0.65)
MWL			LC-M	6.64 (6.66)	0.72 (0.70)
MEN		Globbiomass	NC-M	13.8 (13.8)	0.77 (0.81)
MEL			LC-M	14.5 (14.4)	0.83 (0.87)
GWN	GLC2000	GEOCARBON	NC-M	3.60 (3.62)	0.67 (0.70)
GWL			LC-M	3.81 (3.83)	0.72 (0.75)
GEN		Globbiomass	NC-M	9.04 (9.00)	0.60 (0.63)
GEL			LC-M	9.48 (9.43)	0.65 (0.69)
Average				8.40 (8.39)	0.70 (0.60)

In Table 2, the largest CO_2 emissions value was by MEL at 14.5 ± 0.83 Pg CO_2 year^{-1}, and the smallest was by GWN at 3.60 ± 0.67 Pg CO_2 year^{-1} from 2001 to 2020; MEL showed much larger emissions than GWN by a factor of 4.0. The MEL result was larger by 42%, and the GWN result was smaller by 57% compared to the average emissions. The CO_2 emissions closest to the average emissions were from GEN at 9.04 ± 0.60 Pg CO_2 year^{-1}. The estimated emissions were equivalent to 16–58% of the global carbon budget sourced from fossil fuels and industry from 2001 to 2018 [41].

Figure 4 shows global distribution maps of CO_2 emissions. In the maps, high CO_2 emission areas were central Africa and the Amazon region. However, it is difficult to find differences in distributions among the maps.

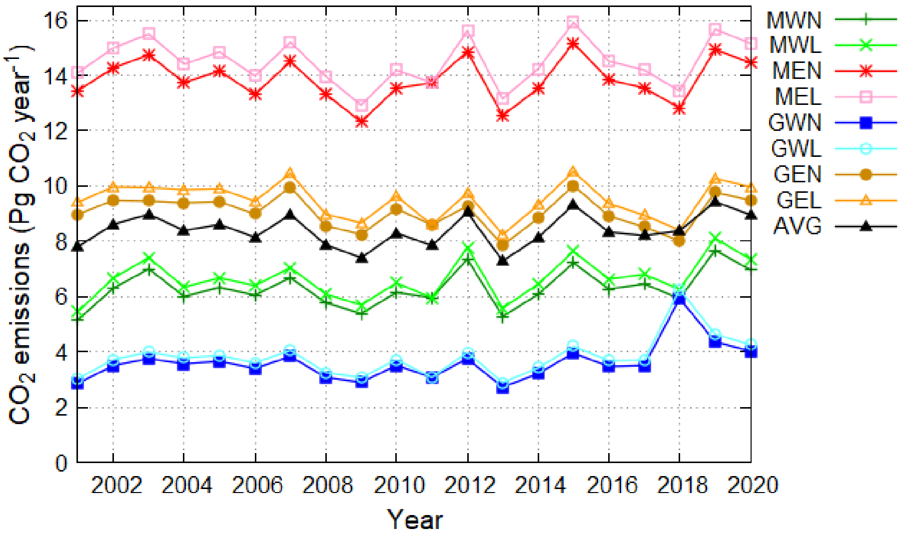

Figure 3. Interannual variation in CO_2 emissions of eight inventories between 2001 and 2020. The datasets used for each inventory are shown in Table 2. AVG denotes the average of the eight inventories.

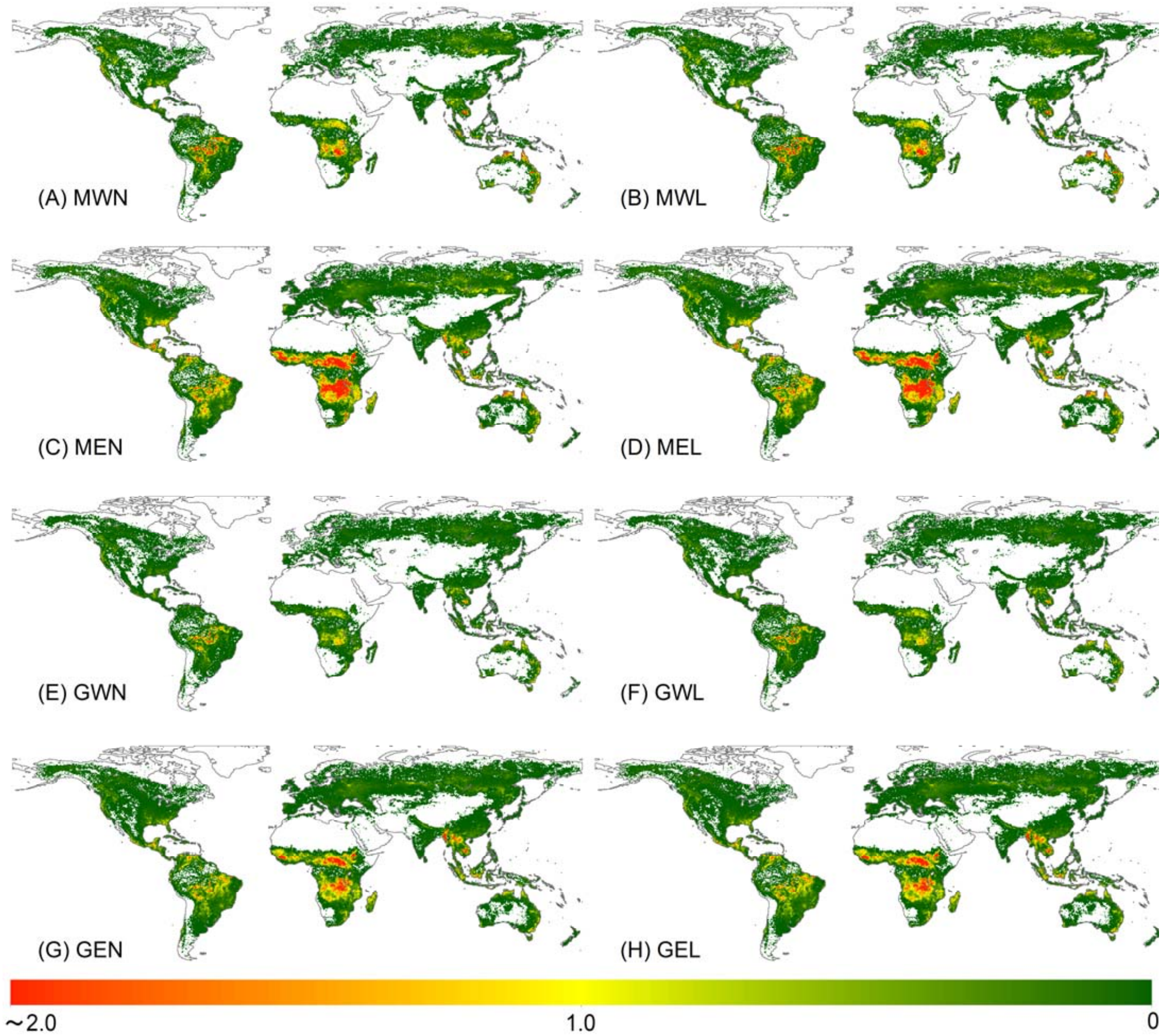

Figure 4. Global maps of average CO_2 emissions (Tg CO_2 grid^{-1} year^{-1}) of the eight inventories from 2001 to 2020. Grid size is 50 km × 50 km.

3.3. Comparison of Annual CO_2 Emissions with Previous Research

The eight inventories of global CO_2 emissions (Table 2) were compared to four inventories (GFED4.1s, GFASv1.2, FINNv1.5, and GICC) of previous studies to assess their validity and variability. The annual CO_2 emission averages from 2003 to 2019 were calculated to match the analysis period for the comparison. The average ($\pm$1 SD) of the annual CO_2 emissions for the four inventories was 7.28 $\pm$ 0.60 Pg CO_2 year^{-1} from 2003 to 2019 (Table 3). In the previous inventories, the largest CO_2 emission was from GICC at 9.64 $\pm$ 0.66 Pg CO_2 year^{-1}, and the smallest was from FINNv1.5 at 5.99 $\pm$ 1.15 Pg CO_2 year^{-1}. The annual CO_2 emission from MWL was 6.66 $\pm$ 0.70 Pg CO_2 year^{-1} from 2003 to 2019 (Table 2), which was 3% larger, 4% smaller, 9% larger, and 31% smaller, respectively, than those from GFASv1.2, GFED4.1s, FINNv1.5, and GICC. The average annual CO_2 emissions from three previous studies, excluding GICC, were within 1 SD of MWL emissions.

Table 3. Average annual CO_2 emissions for the previous studies. Numbers in parentheses are from 2003 to 2019.

Inventory	Period	Average (Pg CO_2 year^{-1})	1 Standard Deviation (Pg CO_2 year^{-1})
GFED4.1s	2001–2019	6.97 (6.93)	0.64 (0.63)
GFASv1.2	2003–2020	6.37 (6.44)	0.72 (0.68)
FINNv1.5	2002–2019	5.99 (6.10)	1.15 (1.09)
GICC	2001–2020	9.64 (9.65)	0.66 (0.65)
Average	2003–2019	7.28	0.60

3.4. Regional Evaluations

We evaluated monthly CO_2 emissions for each of the 14 regions (Figure 1) to understand the regional characteristics and variation. The monthly CO_2 emissions of MWL, MEL, GWL, and GEL are shown in Figure 5. Four inventories from NC-M (MWN, MEN, GWN, and GEN) are not in the figure because the differences between NC-M and LC-M in terms of CO_2 emissions were small (Table 2). In 10 regions, including the global scale, CO_2 emissions were the largest in MEL followed by GEL, MWL, and GWL, respectively, which was similar to the annual emissions (Table 2). However, GEL in SEAS and MWL in AUST showed the largest CO_2 emissions in four inventories, respectively. In Tables 4 and 5, GEL has a larger area and a higher BD in the non-forest areas than MEL in all regions, and the greatest difference (79%) of the BD for non-forest areas was in SEAS. AUST was the only region in which the BD of MWL was higher than that of MEL in the forest areas. These results show that the estimated CO_2 emissions are affected by the input datasets of AGB and LCC.

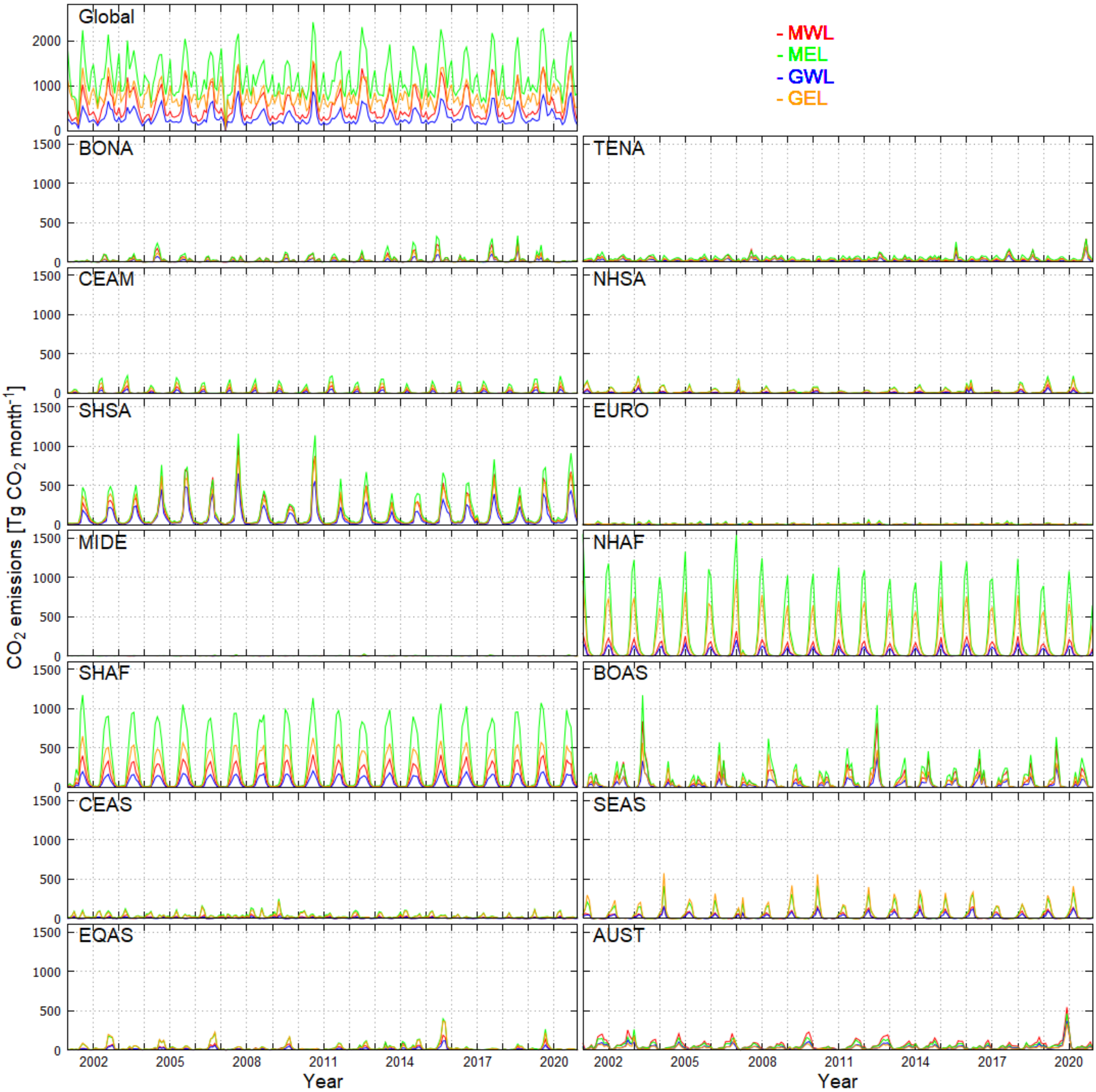

Figure 5. Comparison of the monthly CO_2 emissions by four inventories in each region from January 2001 to December 2020. The compared inventories are MWL (red), MEL (green), GWL (blue), and GEL (orange).

Table 4. Forest and non-forest areas in each region for the LCC maps. Forest and non-forest areas in MCD12Q1 are the averages from 2001 to 2018. Regions of "water," "no-data" categories, and "Antarctica" are excluded.

Region	Forest (10^6 km^2)		Non-Forest (10^6 km^2)	
	MCD12Q1	GLC2000	MCD12Q1	GLC2000
BONA	11.6	9.9	14.2	14.9
TENA	4.1	4.5	7.4	7.0
CEAM	1.7	1.4	1.6	1.9
NHSA	3.0	2.1	0.5	1.4
SHSA	10.5	7.4	7.8	10.8
EURO	5.1	3.8	12.4	13.8
MIDE	0.3	0.3	15.6	15.6
NHAF	4.2	3.2	13.2	14.2
SHAF	5.5	5.0	6.3	6.8
BOAS	19.9	19.8	17.9	18.0
CEAS	5.2	4.3	20.9	23.6
SEAS	2.8	1.9	5.5	6.4
EQAS	2.9	1.9	0.3	1.4
AUST	1.5	1.5	8.9	8.8
Global	78.3	66.8	132.6	144.5

Table 5. Average biomass densities of forest and non-forest areas in each AGB product based on two LCC maps.

Region	Average Biomass Densities (kg m^{-2})							
	Forest				Non-Forest			
	MCD12Q1		GLC2000		MCD12Q1		GLC2000	
	GEOCARBON	Globbiomass	GEOCARBON	Globbiomass	GEOCARBON	Globbiomass	GEOCARBON	Globbiomass
BONA	3.9	6.4	4.6	6.0	0.1	0.6	0.1	1.2
TENA	7.2	10.5	7.5	9.1	0.6	0.9	0.1	1.2
CEAM	3.2	6.9	4.0	6.2	0.2	0.5	0.2	2.1
NHSA	18.8	19.7	25.7	23.6	0.9	2.5	2.3	7.8
SHSA	12.5	14.0	16.2	16.3	0.4	0.9	0.8	2.9
EURO	4.8	8.0	6.4	8.5	0.1	0.5	0.1	1.0
MIDE	3.4	6.8	3.9	5.8	0.0	0.1	0.0	0.1
NHAF	11.6	13.0	14.4	13.6	0.0	0.8	0.2	1.5
SHAF	8.1	10.1	8.5	9.8	0.2	1.8	0.4	2.6
BOAS	4.8	6.5	4.9	6.2	0.2	0.7	0.2	1.2
CEAS	4.0	7.1	5.3	6.9	0.1	0.3	0.1	0.6
SEAS	6.0	10.4	8.6	8.8	0.2	0.5	0.3	2.4
EQAS	19.8	21.0	28.3	22.7	3.7	6.6	4.4	14.4
AUST	11.3	10.4	13.5	9.6	0.5	0.5	0.1	0.6
Global	7.6	9.7	8.7	9.4	0.2	0.6	0.2	1.4

4. Discussions

4.1. Burned Area

The average burned areas of NC-M and LC-M were within 1 SD of CCI50 and outside the SDs of GFED4 and GFED4.1s. One of the causes of the difference in the detected burned area is different data sources for fire detection. In GFED4.1s and GFED4, burned area is detected from MODIS MCD64 collection 5.1 (C5) [6,16]. The burned area of GFED4.1s was 28% larger than that of GFED4 due to the application of the small fire estimation approach [6]. According to Chuvieco et al. (2018) [39], the global annual burned area increased by 27% with the update from MCD64 C5 to MCD64A1 collection 6 (C6) due to improvement in the burned area detection (including small burns), with a reduction in the omission error. Therefore, we consider it reasonable that the burned area of LC-M detected from MCD14A1 C6 was larger than that of GFED4 based on MCD64 C5. However, because there is a non-negligible difference between the FD maps we used and GFED4.1s, a more accurate burned area estimation with small fires is an issue for the future.

4.2. Global CO_2 Emissions Estimation

To know the effect of LCC map on CO_2 emissions, results from the two LCC maps were compared. The CO_2 emissions of MWN and MWL were 43% larger than those of GWN and GWL, respectively, which all use GEOCARBON. Similarly, the CO_2 emissions of MEN and MEL were 35% larger than those of GEN and GEL, respectively, which commonly use Globbiomass. These results show that CO_2 emissions from MCD12Q1 were larger than those of GLC2000. One of the reasons for the high emissions from MCD12Q1 is the differences in the forest area. The forest area on the global scale for MCD12Q1 is approximately 15% larger than that of GLC2000 (Table 4). Furthermore, the forest area of MCD12Q1 is 30–34% larger in the Amazon region (SHSA), with a large number of carbon stocks, and the EQAS region with vast peat swamp forests (Table 4). The differences in the forest area affect the EF and BE are values and cause a large CO_2 emission estimation.

As for the effect of the AGB map, the CO_2 emissions of MWN and MWL were estimated to be 54% smaller than those of MEN and MEL, respectively, which commonly use MCD12Q1. Similarly, the CO_2 emissions of GWN and GWL were 60% smaller than those of GEN and GEL, respectively, which uses GLC2000. These results show that Globbiomass resulted in higher CO_2 emissions than GEOCARBON. The difference is partly because Globbiomass has a larger BD than GEOCARBON in forest and non-forest areas. GEOCARBON is a global forest AGB map, which focused on the forest area and has been evaluated to be 9–18% smaller than its two sources, namely the AGB maps of Saatchi et al. (2011) [33] and Baccini et al. (2012) [34], in the tropical regions [15]. Alternatively, Globbiomass used L-band SAR data, which are used to estimate low biomass from the radar scattering in branches and trunks with penetration of the canopy [42]. These facts are considered as one of the reasons why Globbiomass evaluated AGB to be larger than GEOCARBON and led to a difference in BD of over 50% in non-forest areas (Table 5).

To know the effect of the FD map, two groups using NC-M (MWN, MEN, GWN, and GEN) and LC-M (MWL, MEL, GEL, and GEL) were compared. From the result, NC-M showed 5% smaller CO_2 emissions. The effect of the FD map on CO_2 emissions is smaller than those of LCC and AGB because the difference in the burned area between NC-M and LC-M is small.

4.3. Comparison of Annual CO_2 Emissions with Previous Research

The burned area used to estimate CO_2 emissions contributes to the difference in the emissions in each inventory. GFED4.1s was estimated to have the highest CO_2 emissions in every inventory using the burned area, which is 28% larger than that of GFED4 and 15% larger than that of LC-M, by updating the small fire detection (Figure 2). MOD14 C5, which FINNv1.5 used for the burned area, is the previous version of our burned area product (MOD14A1 C6) with the improvement of detecting small fires and reducing omission errors. The burned area of the previous version is one of the reasons that lead to a lower estimation result than the other inventories, such as MWL and GFED4.1s. GFASv1.2 had less CO_2 emissions than GFED4.1s because GFASv1.2 determined several scaling factors to match the emissions of GFED3.1, which was before the small fire detection update [17]. GICC defines BD as fixed values for each LCC. The BD used in GICC was 18.04 kg m^{-2} for the forest area and 1.35 kg m^{-2} for the non-forest area, which was calculated like Table 5. Although the BD in GLC2000, which was used in GICC, was lower than those of GEOCARBON and Globbiomass in non-forest areas, it was higher in forest areas by 277% and 236% for GEOCARBON and Globbiomass, respectively, which has a greater effect on CO_2 emissions estimates.

4.4. Regional Evaluations

Eight inventories are compared with the results of previous papers to evaluate the regional CO_2 emissions. Guo et al. (2017) [43] reported CO_2 emissions from wildfires in western Russia from July to August 2010 to be 255 Tg CO_2 using GOSAT satellite observation data. Assuming that wildfire is a dominant source in this period in the BOAS region, the MWL inventory (248 Tg CO_2) is the closest value among the eight inventories. The BD difference in AGB maps is influenced by the fire emissions because the difference between the forest and the non-forest areas in the two LCC maps was small in BOAS (Table 4). Huijnen et al. (2016) [44] estimated CO_2 emissions from fires in Southeast Asia (EQAS for our evaluation) from September to October 2015 to be 692 Tg CO_2 based on the in situ observed EF ratios. The closest inventory to this value was MEN (702 Tg CO_2), which used MCD12Q1 with a larger forest area than GLC2000 (Table 4) and Globbiomass, with higher BD values than GEOCARBON in both the forest and non-forest areas (Table 5). There is the possibility that the input sources for the estimation have regional uncertainty. Although it is difficult to make a quantitative conclusion for the small number of evaluation samples, the inventories using MCD12Q1 with a larger forest area than GLC2000 may tend to be close to the fire CO_2 emissions of previous studies. In AGB, GEOCARBON has closed fire emissions of several previous studies, globally. The reason for this closure is because previous studies (e.g., GFASv1.2) fixed their scaling factors to estimate the fire emissions based on GFED, and GFED uses GEOCARBON for adjusting the AGB as one of the input sources of the CASA model, which is the basis for calculating the carbon pools [6]. The two AGB maps used in our estimation differ in the non-forest areas, and Globbiomass has a larger BD (Table 5). From the results, when a survey region for the fire emission estimation is in a non-forest area with a relatively large BD, such as a tropical region, Globbiomass may contribute to the estimation. However, an accurate evaluation of fire emissions needs to be analyzed to compare with the atmospheric concentrations in the future.

4.5. Evaluation of Estimation Method

The new estimation method of CO_2 emission, incorporating the arranged BD by the number of fire occurrences (Equation (2)), was compared with the general burned area approach (Equation (1)). The MWL inventory and GFED4.1s were used for comparison because they use common input data sources, and GFED4.1s is one of the most standard inventories of fire emissions. The average annual CO_2 emissions of the conventional and new methods were 6.31 ± 0.65 and 6.60 ± 0.72 Pg CO_2 $year^{-1}$, respectively, which were 9.6% and 5.4% smaller, respectively, than that of GFED4.1s (Figure S3). There was a statistically significant difference in each population average between the conventional and new methods under a one-sided *t*-test at a 5% significance level. These results show that the amount estimated using the new method was approximately 4% closer to GFED4.1s in the CO_2 emission estimations compared with the conventional method; this result is attributed to the arrangement of BD by the number of fire occurrences.

4.6. Uncertainty

The uncertainty in our estimation method was from remote sensing data, scaling coefficients, and features of this method itself in fire term and scale. FD, LCC, and AGB maps used in the estimation also have their uncertainties. Hawbaker et al. (2008) [45] reported that small fires and cloud cover led to decreased fire detection, and MOD14A1 has an overall fire detection rate of 82%. In the LCC map, GLC2000 had overall accuracies of 68.6% [46], and Sulla-Menashe et al. (2019) [31] reported an overall accuracy of 73.6% for MCD12Q1. However, because accuracy depends on the change in the LCC category, location, and burning time, these can lead to complex uncertainties. Avitabile et al. (2016) [15] reported that GEOCARBON has a root mean square error (RMSE) of 87–98 Mg ha^{-1}, whereas ESA (2017) [35] reported that Globbiomass has an RMSE of 48.2–80.0 Mg ha^{-1} in Africa, South America, and Asia. These differences in accuracy produce bigger BD variations from expanding the target region to a global scale and distinguishing forest and non-forest areas, as shown in Table 2. An accurate understanding of changing BD due to changing land cover type is difficult because the AGB maps do not have time-series data. Although we assigned EF and BE to each land cover category based on past papers, their actual values are highly variable depending on region, season, and weather [47,48]. Hoelzemann et al. (2004) [49] stated that the uncertainty of EF is in the order of 20–30% and that of BEs is 12% in savannas and grasslands and 20% in forests. Furthermore, van der Werf et al. (2017) [6] mentioned that EF has a variation of approximately 40% on average, and diurnal or long-term variation in EF should be larger. Shiraishi and Hirata (in press) [38] reported that the results of CO_2 emission estimation using local scaling factors were 1.8 times higher than those of global scaling factors as same values with this paper in Australia.

Uncertain factors in our estimation method included burning term and scale. Our method uses a one-time fire instance for estimation and does not consider burning term or fire scale. Thus, fires that continue to burn for multiple days carry equal weight as one-day fires. Although the BD incinerated monthly and annually is considered by Equation (2), biomass growth and recovery are not considered. These uncertainties influence each other and complicate evaluations of estimation results.

Concrete uncertainty was not mentioned in the previous study. van der Werf et al. (2010) [5] estimated a 20% uncertainty for GFED3 by applying a Monte Carlo simulation to the estimation model. However, van der Werf et al. (2017) [6] reported that it is difficult to estimate uncertainty for GFED4, partly because it is difficult to evaluate the uncertainties of parameters and layers defined for the simulation. Although FINN reported that uncertainties were approximately twice of the estimated emissions, Wiedinmyer et al. (2011) [22] concluded that uncertainties are difficult to assign quantitatively because of uncertainties associated with LCCs, fire detection, burned area assumption, biomass loading, amount of fuel burned, and emission factors.

FINN had its uncertainties concluded compared with CO emissions by air pollutant emissions inventories of the United States Environmental Protection Agency (EPA) [50]. However, it should be noted that the EPA observations are not for global data but rather for the United States. CO is considered a useful biomass burning tracer [51], and uncertainties associated with biomass burning estimates can be tested using CO [2]. As was the case with FINN, we evaluated CO emissions of the eight input datasets using EPA CO emissions. This method for estimating CO emissions involves Equations (1) and (2), and the EF, which was assigned for the LCC categories in this study, as shown in Table S3 for MCD12Q1 and Table S4 for GLC2000. The average (with 1 SD) of the eight CO emissions was 17.5 ± 4.19 Tg CO $year^{-1}$, and the result depended on the input datasets, like the CO_2 emissions (Figure 6 and Table S5). CO emissions of the four inventories using Globbiomass (MEN, MEL, GEN, and GEL) were 36–44% greater than those of GEOCARBON (MWN, MWL, GWN, and GWL). The results are influenced by BD in the forest area, as shown in Table S6. The average CO emissions from EPA was 12.9 ± 3.86 Tg CO $year^{-1}$, and the closest emission was found by GWL at 10.5 ± 3.45 Tg CO $year^{-1}$, which was smaller by 18% compared with that of EPA. If we perform the same evaluation as in Wiedinmyer et al. (2011) [22], then, it is possible to conclude that the uncertainty in GWL is at least 18% in TENA. However, it is not possible to conclude the uncertainties of the whole inventory by comparing CO emissions within limited areas. As shown in Figure 4, most of the CO_2 emissions were in

Africa and South America, thus evaluating these areas, where CO_2 emissions are higher, is indispensable. In addition, because LCC categories and BDs differ by continent and region, uncertainties cannot be determined by evaluating TENA alone. The comparison of CO emissions for the uncertainty evaluation in other continents, especially high BD and frequently fired regions, needs to be analyzed.

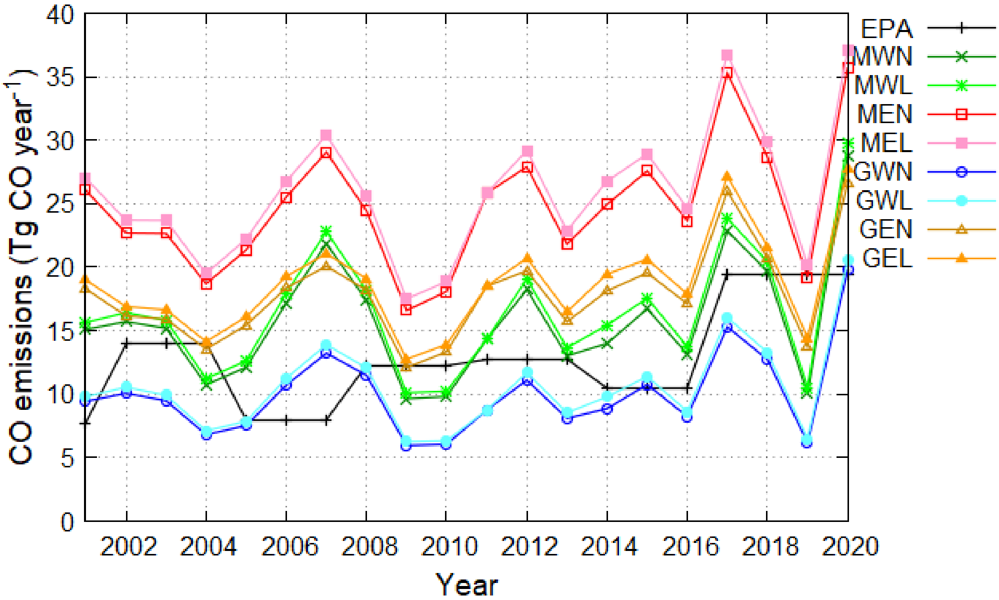

Figure 6. Comparison of CO emissions between EPA and estimated eight results in the United States.

5. Conclusions

This study presented eight global and regional CO_2 emission inventories through biomass burning, the uncertainty assessments of fire emission estimation from input datasets, and comparing results between created inventories and the previous four inventories from 2001 to 2020. Global annual CO_2 emissions of the four previous inventories were within 1 SD from the average CO_2 emissions in any of created eight inventories. We found that among the eight inventories, MWL, which used MCD12Q1 for LCC, GEOCARBON for AGB, and LC-M for FD, showed the closest CO_2 emissions at global scale. Furthermore, the inventories using MCD12Q1 and Globbiomass were close to the emissions of previous studies in the survey area, including the non-forest areas with a relatively high BD. However, it is difficult to specify the uncertainty of each inventory as in the previous studies.

We found how more detailed FD, LCC, and BD maps can reduce uncertainty in fire CO_2 emissions inventories proposed in this study. The used biomass maps were single-year datasets, and the continuous temporal variation in the BD was not considered in the method. Geographical and meteorological variations of BE and EF, and the use of higher-spatial-resolution products for input datasets, should be considered. Although remote sensing products available for fire emission estimation are increasing, estimations using new products are a future topic. The CO_2 emissions inventories in this study will be opened. We expect that the inventories can provide new choices to users and its estimation by input sources help to assess the performance of climate and fire models.

Supplementary Materials: The following are available online at https://www.mdpi.com/article/10.3390/rs13101914/s1, Figure S1: Global burned area trend of two fire distribution maps, Figure S2: Regional burned area trend for LC-M, Figure S3: Comparison of the estimated CO_2 emissions using new and conventional methods, Table S1: Abbreviation list, Table S2: Burning efficiency and emission factors for forest and non-forest in GLC2000 and MCD12Q1, Table S3: Emission factors for CO based on MCD12Q1, Table S4: Emission factors for CO based on GLC2000, Table S5: Averages of annual CO emissions, Table S6: Comparison of the average biomass density.

Author Contributions: Conceptualization, R.H.; methodology, R.H. and T.S.; software, T.S.; validation, T.S.; formal analysis, T.S.; investigation, T.S.; resources, T.S.; data curation, T.S.; writing—original draft preparation, T.S.; writing—review and editing, R.H. and T.H.; visualization, T.S.; supervision, R.H and T.H.; project administration, R.H.; funding acquisition, R.H. All authors have read and agreed to the published version of the manuscript.

Funding: This study was partially supported by the GOSAT-2 Project at the National Institute for Environmental Studies (NIES) and the Climate Change Adaptation Research Program of NIES.

Data Availability Statement: The data presented in this study are openly available in MOD14A1 and MCD12Q1 products, the NASA EOSDIS Land Processes Distributed Active Archive Center (LP DAAC) at the USGS Earth Resources Observation and Science (EROS) Center, Sioux Falls, South Dakota at https://lpdaac.usgs.gov (accessed on 12 March 2021). Globbiomass map at http://globbiomass.org/products/global-mapping (accessed on 12 March 2021). GEOCARBON global forest biomass map was downloaded at http://lucid.wur.nl/datasets/high-carbon-ecosystems (accessed on 12 March 2021). The air emissions inventory in United States for CO download from EPA at https://www.epa.gov/air-emissions-inventories (accessed on 12 March 2021).

Conflicts of Interest: The authors declare no conflict of interest.

References

1. Neto, T.G.S.; Carvalho, J.A.; Veras, C.A.G.; Alvarado, E.C.; Gielow, R.; Lincoln, E.N.; Christian, T.J.; Yokelson, R.J.; Santos, J.C. Biomass consumption and CO_2, CO and main hydrocarbon gas emissions in an Amazonian forest clearing fire. *Atmos. Environ.* **2009**, *43*, 438–446. [CrossRef]
2. Kaiser, J.W.; Heil, A.; Andreae, M.O.; Benedetti, A.; Chubarova, N.; Jones, L.; Morcrette, J.J.; Razinger, M.; Schultz, M.G.; Suttie, M.; et al. Biomass burning emissions estimated with a global fire assimilation system based on observed fire radiative power. *Biogeosciences* **2012**, *9*, 527–554. [CrossRef]
3. Lin, N.H.; Tsay, S.C.; Maring, H.B.; Yen, M.C.; Sheu, G.R.; Wang, S.H.; Chi, K.H.; Chuang, M.T.; Ou-Yang, C.F.; Fu, J.S.; et al. An overview of regional experiments on biomass burning aerosols and related pollutants in Southeast Asia: From BASE-ASIA and the Dongsha Experiment to 7-SEAS. *Atmos. Environ.* **2013**, *78*, 1–19. [CrossRef]
4. Van der Werf, G.R.; Randerson, J.T.; Giglio, L.; Collatz, G.J.; Kasibhatla, P.S.; Arellano, A.F. Interannual variability in global biomass burning emissions from 1997 to 2004. *Atmos. Chem. Phys.* **2006**, *6*, 3423–3441. [CrossRef]
5. Van der Werf, G.R.; Randerson, J.T.; Giglio, L.; Collatz, G.J.; Mu, M.; Kasibhatla, P.S.; Morton, D.C.; Defries, R.S.; Jin, Y.; Van Leeuwen, T.T. Global fire emissions and the contribution of deforestation, savanna, forest, agricultural, and peat fires (1997–2009). *Atmos. Chem. Phys.* **2010**, *10*, 11707–11735. [CrossRef]
6. Van der Werf, G.R.; Randerson, J.T.; Giglio, L.; Van Leeuwen, T.T.; Chen, Y.; Rogers, B.M.; Mu, M.; Van Marle, M.J.E.; Morton, D.C.; Collatz, G.J.; et al. Global fire emissions estimates during 1997–2016. *Earth Syst. Sci. Data* **2017**, *9*, 697–720. [CrossRef]
7. Chen, Y.; Randerson, J.T.; Morton, D.C.; Defries, R.S.; Collatz, G.J.; Kasibhatla, P.S.; Giglio, L.; Jin, Y.; Marlier, M.E. Forecasting Fire Season Severity in South America Using Sea Surface Temperature Anomalies. *Science* **2011**, *334*, 787–791. [CrossRef]
8. van der Werf, G.R.; Morton, D.C.; Defries, R.S.; Olivier, J.G.J.; Kasibhatla, P.S.; Jackson, R.B.; Collatz, G.J.; Randerson, J.T. CO_2 emissions from forest loss. *Nat. Geosci.* **2009**, *2*, 737–738. [CrossRef]
9. Morton, D.C.; Defries, R.S.; Randerson, J.T.; Giglio, L.; Schroeder, W.; van der Werf, G.R. Agricultural intensification increases deforestation fire activity in Amazonia. *Glob. Chang. Biol.* **2008**, *14*, 2262–2275. [CrossRef]
10. Radke, L.F.; Stith, J.L.; Hegg, D.A.; Hobbs, P.V. Airborne Studies of Particles and Gases from Forest Fires. *J. Air Pollut. Control Assoc.* **1978**, *28*, 30–34. [CrossRef]
11. Seiler, W.; Crutzen, P.J. Estimates of Gross and Net Fluxes of Carbon Between. *Clim. Chang.* **1980**, *2*, 207–247. [CrossRef]
12. Duncan, B.N. Interannual and seasonal variability of biomass burning emissions constrained by satellite observations. *J. Geophys. Res.* **2003**, *108*. [CrossRef]
13. van der Werf, G.R.; Randerson, J.T.; Collatz, G.J.; Giglio, L.; Kasibhatla, P.S.; Arellano, A.F., Jr.; Olsen, S.C.; Kasischke, E.S. Continental-Scale Partitioning of Fire Emissions During the 1997 to 2001 El Niño/La Niña Period. *Science* **2004**, *303*, 73–77. [CrossRef] [PubMed]
14. Ge, Y.; Avitabile, V.; Heuvelink, G.B.M.; Wang, J.; Herold, M. Fusion of pan-tropical biomass maps using weighted averaging andregional calibration data. *Int. J. Appl. Earth Obs. Geoinf.* **2014**, *31*, 13–24. [CrossRef]
15. Avitabile, V.; Herold, M.; Heuvelink, G.B.M.; Lewis, S.L.; Phillips, O.L.; Asner, G.P.; Armston, J.; Ashton, P.S.; Banin, L.; Bayol, N.; et al. An integrated pan-tropical biomass map using multiple reference datasets. *Glob. Chang. Biol.* **2016**, *22*, 1406–1420. [CrossRef]
16. Giglio, L.; Randerson, J.T.; van der Werf, G.R. Analysis of daily, monthly, and annual burned area using the fourth-generation global fire emissions database (GFED4). *J. Geophys. Res. Biogeosci.* **2013**, *118*, 317–328. [CrossRef]
17. Rémy, S.; Veira, A.; Paugam, R.; Sofiev, M.; Kaiser, J.W.; Marenco, F.; Burton, S.P.; Benedetti, A.; Engelen, R.J.; Ferrare, R.; et al. Two global data sets of daily fire emission injection heights since 2003. *Atmos. Chem. Phys.* **2017**, *17*, 2921–2942. [CrossRef]

18. Di Giuseppe, F.; Rémy, S.; Pappenberger, F.; Wetterhall, F. Using the Fire Weather Index (FWI) to improve the estimation of fire emissions from fire radiative power (FRP) observations. *Atmos. Chem. Phys.* **2018**, *18*, 5359–5370. [CrossRef]
19. Bartalev, S.A.; Belward, A.S.; Erchov, D.V.; Isaev, A.S. A new SPOT4-VEGETATION derived land cover map of Northern Eurasia. *Int. J. Remote Sens.* **2003**, *24*, 1977–1982. [CrossRef]
20. Bartholomé, E.; Belward, A.S. GLC2000: A new approach to global land cover mapping from earth observation data. *Int. J. Remote Sens.* **2005**, *26*, 1959–1977. [CrossRef]
21. Wiedinmyer, C.; Quayle, B.; Geron, C.; Belote, A.; McKenzie, D.; Zhang, X.; O'Neill, S.; Wynne, K.K. Estimating emissions from fires in North America for air quality modeling. *Atmos. Environ.* **2006**, *40*, 3419–3432. [CrossRef]
22. Wiedinmyer, C.; Akagi, S.K.; Yokelson, R.J.; Emmons, L.K.; Al-Saadi, J.A.; Orlando, J.J.; Soja, A.J. The Fire INventory from NCAR (FINN): A high resolution global model to estimate the emissions from open burning. *Geosci. Model. Dev.* **2011**, *4*, 625–641. [CrossRef]
23. Arino, O.; Muriel, S.; Piccolini, I.; Rosaz, J.M. The ers-2 atsr-2 world fire atlas and the ers-2 atsr-2 world burnt surface atlas projects. In Proceedings of the 8th ISPRS Conference on Physical Measurement and Signatures in Remote Sensing, Aussois, France, 8–12 January 2001.
24. Tansey, K.; Grégoire, J.-M.; Binaghi, E.; Boschetti, L.; Brivio, P.A.; Ershov, D.; Flasse, S.; Fraser, R.; Graetz, D.; Maggi, M.; et al. A global inventory of burned areas at 1 km resolution for the year 2000 derived from spot vegetation data. *Clim. Chang.* **2004**, *67*, 345–377. [CrossRef]
25. Mieville, A.; Granier, C.; Liousse, C.; Guillaume, B.; Mouillot, F.; Lamarque, J.F.; Grégoire, J.M.; Pétron, G. Emissions of gases and particles from biomass burning during the 20th century using satellite data and an historical reconstruction. *Atmos. Environ.* **2010**, *44*, 1469–1477. [CrossRef]
26. Shi, Y.; Matsunaga, T.; Saito, M.; Yamaguchi, Y.; Chen, X. Comparison of global inventories of CO_2 emissions from biomass burning during 2002-2011 derived from multiple satellite products. *Environ. Pollut.* **2015**, *206*, 479–487. [CrossRef]
27. Justice, C.; Giglio, L.; Boschetti, L.; Roy, D.; Csiszar, I. *Algorithm Technical Background Document*; NASA: Washington, DC, USA, 2006.
28. Giglio, L.; Schroeder, W.; Justice, C.O. The collection 6 MODIS active fire detection algorithm and fire products. *Remote Sens. Environ.* **2016**, *178*, 31–41. [CrossRef] [PubMed]
29. Giglio, L. *MODIS Collection 6 Active Fire Product User's Guide Revision A*; Department of Geographical Sciences, NASA: Washington, DC, USA, 2015. [CrossRef]
30. Strahler, A.; Gopal, S.; Lambin, E.; Moody, A. *MODIS Land Cover Product Algorithm Theoretical Basis Document (ATBD) Version 5.0*; NASA: Washington, DC, USA, 1999.
31. Sulla-Menashe, D.; Gray, J.M.; Abercrombie, S.P.; Friedl, M.A. Hierarchical mapping of annual global land cover 2001 to present: The MODIS Collection 6 Land Cover product. *Remote Sens. Environ.* **2019**, *222*, 183–194. [CrossRef]
32. Santoro, M.; Cartus, O.; Mermoz, S.; Bouvet, A.; Le Toan, T.; Carvalhais, N.; Rozendaal, D.; Herold, M.; Avitabile, V.; Quegan, S.; et al. A detailed portrait of the forest aboveground biomass pool for the year 2010 obtained from multiple remote sensing observations. Geophysical Research Abstracts, 20, EGU2018-18932. *Geophys. Res.* **2018**, *20*, 18932.
33. Saatchi, S.S.; Harris, N.L.; Brown, S.; Lefsky, M.; Mitchard, E.T.A.; Salas, W.; Zutta, B.R.; Buermann, W.; Lewis, S.L.; Hagen, S.; et al. Benchmark map of forest carbon stocks in tropical regions across three continents. *Proc. Natl. Acad. Sci. USA* **2011**, *108*, 9899–9904. [CrossRef]
34. Baccini, A.; Goetz, S.J.; Walker, W.S.; Laporte, N.T.; Sun, M.; Sulla-Menashe, D.; Hackler, J.; Beck, P.S.A.; Dubayah, R.; Friedl, M.A.; et al. Estimated carbon dioxide emissions from tropical deforestation improved by carbon-density maps. *Nat. Clim. Chang.* **2012**, *2*, 182–185. [CrossRef]
35. European Space Agency. *DUE GlobBiomass Validation Report*; European Space Agency: Darmstadt, Germany, 2017.
36. Quegan, S.; Rauste, Y.; Bouvet, A.; Carreiras, J.; Cartus, O.; Carvalhais, N.; LeToan, T.; Mermoz, S.; Santoro, M. *D6–Global Biomass Map Algorithm Theoretical Basis Document (Incorporating the Design Justification File D7)*; European Space Agency: Darmstadt, Germany, 2017.
37. Michel, C.; Liousse, C.; Grégoire, J.M.; Tansey, K.; Carmichael, G.R.; Woo, J.H. Biomass burning emission inventory from burnt area data given by the SPOT-VEGETATION system in the frame of TRACE-P and ACE-Asia campaigns. *J. Geophys. Res. D Atmos.* **2005**, *110*, 1–15. [CrossRef]
38. Shiraishi, T.; Hirata, R. Estimation of carbon dioxide emissions from the megafires of Australia in 2019–2020. *Sci. Rep.* **2021**, *11*, 8267. [CrossRef] [PubMed]
39. Chuvieco, E.; Lizundia-Loiola, J.; Pettinari, M.L.; Ramo, R.; Padilla, M.; Tansey, K.; Plummer, S.; Mouillot, F.; Laurent, P.; Storm, T.; et al. Generation and analysis of a new global burned area product based on MODIS 250 m reflectance bands and thermal anomalies. *Earth Syst. Sci. Data* **2018**, *10*, 2015–2031. [CrossRef]
40. Andela, N.; Morton, D.C.; Giglio, L.; Chen, Y.; van der Werf, G.R.; Kasibhatla, P.S.; DeFries, R.S.; Collatz, G.J.; Hantson, S.; Kloster, S.; et al. A humandriven decline in global burned area. *Science* **2017**, *356*, 1356–1362. [CrossRef] [PubMed]
41. Global Carbon Project. *Supplemental Data of Global Carbon Budget 2019 (Version 1.0)*; Global Carbon Project: Canberra, Australia, 2019. [CrossRef]

42. Lucas, R.; Armston, J.; Fairfax, R.; Fensham, R.; Accad, A.; Carreiras, J.; Kelley, J.; Bunting, P.; Clewley, D.; Bray, S.; et al. An Evaluation of the ALOS PALSAR L-Band Backscatter—Above Ground Biomass Relationship Queensland, Australia: Impacts of Surface Moisture Condition and Vegetation Structure. *IEEE J. Sel. Top. Appl. Earth Obs. Remote Sens.* **2010**, *3*, 576–593. [CrossRef]
43. Guo, M.; Li, J.; Xu, J.; Wang, X.; He, H.; Wu, L. CO_2 emissions from the 2010 Russian wildfires using GOSAT data. *Environ. Pollut.* **2017**, *226*, 60–68. [CrossRef]
44. Huijnen, V.; Wooster, M.J.; Kaiser, J.W.; Gaveau, D.L.A.; Flemming, J.; Parrington, M.; Inness, A.; Murdiyarso, D.; Main, B.; Van Weele, M. Fire carbon emissions over maritime southeast Asia in 2015 largest since 1997. *Sci. Rep.* **2016**, *6*, 1–8. [CrossRef]
45. Hawbaker, T.J.; Radeloff, V.C.; Syphard, A.D.; Zhu, Z.; Stewart, S.I. Detection rates of the MODIS active fire product in the United States. *Remote Sens. Environ.* **2008**, *112*, 2656–2664. [CrossRef]
46. Mayaux, P.; Eva, H.; Gallego, J.; Strahler, A.H.; Herold, M.; Member, S.; Agrawal, S.; Naumov, S.; Miranda, E.E.D.; Bella, C.M.D.; et al. Validation of the Global Land Cover 2000 Map. *IEEE Trans. Geosci. Remote Sens.* **2006**, *44*, 1728–1739. [CrossRef]
47. Andreae, M.O.; Merlet, P. Emission of trace gases and aerosols from biomass burning. *Glob. Biogeochem. Cycles* **2001**, *15*, 955–966. [CrossRef]
48. Akagi, S.K.; Yokelson, R.J.; Wiedinmyer, C.; Alvarado, M.J.; Reid, J.S.; Karl, T.; Crounse, J.D. Emission factors for open and domestic biomass burning for use in atmospheric models. *Atmos. Chem. Phys. Emiss.* **2011**, 4039–4072. [CrossRef]
49. Hoelzemann, J.J.; Schultz, M.G.; Brasseur, G.P.; Granier, C.; Simon, M. Global Wildland Fire Emission Model (GWEM): Evaluating the use of global area burnt satellite data. *J. Geophys. Res.* **2004**, *109*, D14S04. [CrossRef]
50. CASTNET: U.S. Environmental Protection Agency Clean Air Markets Division Clean Air Status and Trends Network. Available online: https://www.epa.gov/castnet (accessed on 12 March 2021).
51. Shan, C.; Wang, W.; Liu, C.; Sun, Y.; Hu, Q.; Xu, X.; Tian, Y.; Zhang, H.; Morino, I.; Gri, D.W.T.; et al. Regional CO emission estimated from ground-based remote sensing at Hefei site, China. *Atmos. Res.* **2019**, *222*, 25–35. [CrossRef]